ELSEVIER

Probabilistic Engineering Mechanics 18 (2003) 289–299

PROBABILISTIC ENGINEERING MECHANICS

www.elsevier.com/locate/probengmech

Evolution of crystallographic orientations in crystals subject to random and deterministic deformation

Sanjay R. Arwade[a,*], Mircea Grigoriu[b]

[a]*Department of Civil Engineering, Johns Hopkins University, Baltimore, MD 21202, USA*
[b]*School of Civil and Environmental Engineering, Cornell University, Ithaca, NY 14850, USA*

Received 10 March 2003; revised 16 June 2003; accepted 16 June 2003

Abstract

The response of polycrystals to deterministic and random deformations is investigated with respect to the evolution of the crystallographic orientation and its probability density function, the ODF. The crystals analyzed are highly simplified, being two-dimensional and with only two active slip systems. A differential equation is derived which governs the evolution of the orientation under arbitrary applied inelastic deformation. Evolution of the ODF is analyzed by either solution of a Fokker-Planck equation or Monte Carlo simulation. Two main results are presented. Applied deformation tends to reduce heterogeneity of polycrystals with an initially uniform ODF. The presence of randomness in the applied deformation leads the ODF to evolve to forms which are not obtained under any form of deterministic deformation.

Keywords: Crystallographic orientation; Random processes; Fokker-Planck equation; Material heterogeneity

1. Introduction

The role which material microstructure plays in determining the performance of engineering materials is increasingly being recognized by the engineering community. The goal of the work presented here is to determine the effect of uncertainty in applied loads on the evolution of the atomic lattice orientation in crystalline solids. The atomic lattice orientation is also called the crystallographic orientation.

The crystallographic orientation is determined by the positions of the constituent atoms of a crystalline solid, and, in turn, determines the alignment of the axes of material anisotropy in individual grains. The orientation varies randomly from grain to grain, and therefore the mechanical response of crystalline materials is random, and dependent on the crystallographic orientation.

Many engineering materials, such as aluminum and silicon, are crystalline in structure. The volumes of material typical of engineering applications consist of many grains, and are called polycrystalline. The shape and size of the grains, as well as their orientations, are random and heterogeneous. This random heterogeneity affects mechanical phenomena such as the initiation and growth of microcracks.

An interesting feature of the orientation is that it can evolve during deformation. When a crystalline solid is deformed inelastically, the orientation changes, dependent upon the details of the applied deformation. Since the orientation is random, a probability density function (PDF) can be defined for the orientation. This PDF is called the orientation distribution function (ODF). It is the change, or evolution, of the orientation and ODF which is examined here.

The presentation is made into two main parts. First, the crystalline system is described. The crystal is assumed to be two-dimensional and to have only two active slip systems so that a differential equation can be derived which governs the evolution of the orientation in a material subject to an arbitrary applied deformation. Second, this equation is solved to analyze the evolution of the orientation for a variety of different deformation types, both deterministic and random. The analysis is accomplished by Monte Carlo simulation and by the derivation and solution of a Fokker-Planck equation for the orientation.

A significant body of work exists which addresses the evolution of crystallographic orientation during inelastic

* Corresponding author. Tel.: +1-410-516-7138; fax: +1-410-516-7473.
E-mail address: srarwade@jhu.edu (S.R. Arwade).

0266-8920/03/$ - see front matter © 2003 Elsevier Ltd. All rights reserved.
doi:10.1016/S0266-8920(03)00032-8

deformation [1–10]. In all cases the analysis is performed for deterministic applied deformation. Existing results address both two- and three-dimensional crystals. Only in a few cases has uncertainty in the deformation been addressed [11–13].

2. System definition and mechanical model

The mechanics of crystal plasticity are now described in a general way, while at the same time more precise definitions than given in Section 1 are provided for many of the terms and quantities utilized in the following sections of the paper. Fig. 1 shows a schematic illustration of a crystal lattice in which the circles represent atoms. The lines are included merely for clarity of the figure rather than to explicitly represent interatomic bonds. Also shown are the orthogonal coordinate axes $O(x_1, x_2, x_3)$ which are attached to the crystal lattice. The orientation gives the rotational relationship of this coordinate system to a fixed reference coordinate system. The orientation in a three-dimensional setting has many equivalent representations. It can be given, for example, as the components of a rotation tensor, as the triplet of Euler angles, or as an axis/angle pair [14]. The ODF is simply the PDF of the orientation. The ODF is in general multi-variate.

2.1. Assumptions

In an actual polycrystalline material, as depicted in Fig. 2, the individual grains must interact if the deformation of the body is to satisfy the compatibility conditions placed on deformations and strains. This interaction affects the stress and strain fields in the polycrystal. Since the evolution of orientation is governed partially by the strain, this interaction between grains affects the orientation evolution. Exact solution of the problem while accounting for these interactions is not possible. While approximate numerical solutions can be obtained, solution by this method is very time consuming and computationally expensive.

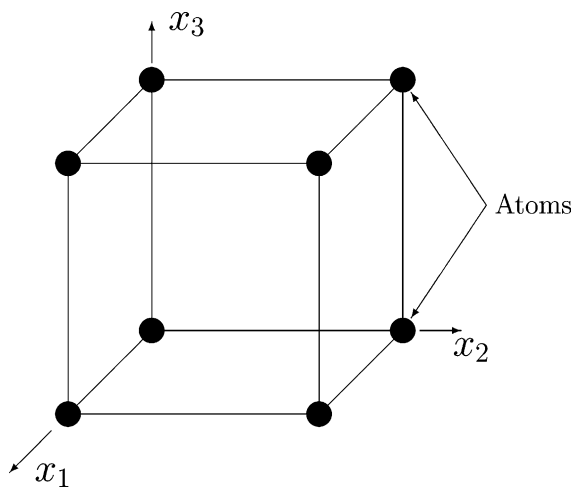

Fig. 1. Schematic illustration of a crystal lattice structure, showing also a possible definition of the crystal coordinate system used in defining the orientation.

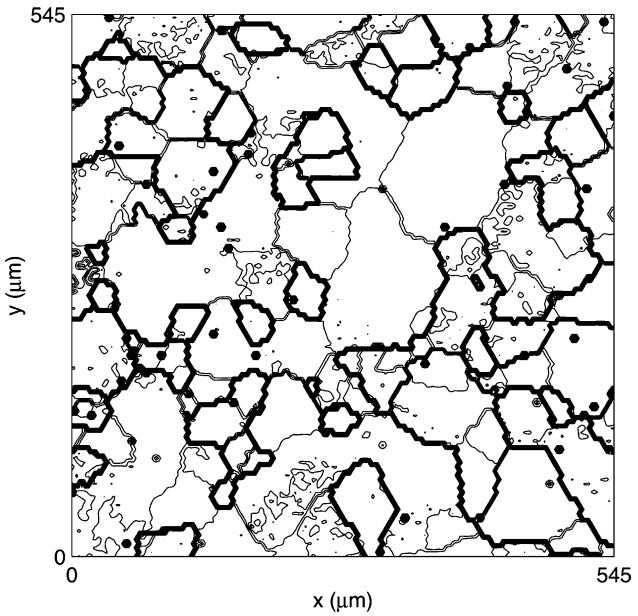

Fig. 2. Contour plot of the experimentally measured crystallographic orientation of AL2024 [18]. The location of the contour lines indicates the change in orientation which occurs at grain boundaries.

The analysis presented here is therefore performed under two simplifying assumptions. The first is the commonly applied Taylor assumption [3,8]. The Taylor assumption states that all crystals in a polycrystal experience identical deformation. This deformation is equal to the specified macroscopic applied deformation. By this assumption compatibility of the polycrystal strains is assured, while violation of equilibrium is allowed. The second assumption is that the applied deformation is accommodated in the polycrystal entirely by inelastic processes. That is, any elastic part of the deformation is neglected. This assumption is appropriate to the analysis for two reasons: orientation evolution is not influenced by elastic deformation, and the magnitude of elastic deformation in problems of interest is small compared to the magnitude of the inelastic deformation.

Two additional assumptions allow the derivation of a closed form governing equation for the orientation, and also make exact solution possible in certain cases. These assumptions are that crystals are planar, or two-dimensional, and that each crystal has only two slip systems available for accommodating inelastic deformation.

2.2. Crystal geometry

Fig. 3 shows the slip system geometry of a planar crystal with two slip systems. The slip systems are defined by vectors $\mathbf{n}^{(k)}$, $k = 1, 2$ normal to the slip plane and slip directions $\mathbf{s}^{(k)}$, $k = 1, 2$. The slip directions differ by the angle 2θ. Deformation of the crystal is accommodated by

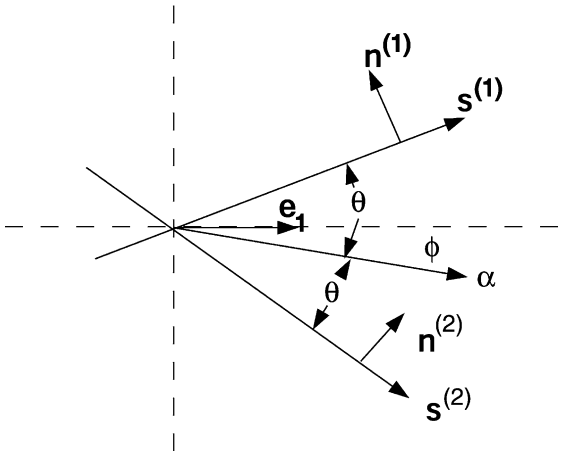

Fig. 3. Geometry of a two-dimensional crystal with two active slip systems.

sliding along the slip planes. The rate of sliding along slip plane k is denoted by $\dot{\gamma}^{(k)}$, the slip system shear rate. The slip system shear rate $\dot{\gamma}^{(k)}$ is positive if sliding is in the direction of the slip direction $\mathbf{s}^{(k)}$.

The vector $\boldsymbol{\alpha}$ is the bisector of the slip directions. The orientation angle ϕ is the angle between $\boldsymbol{\alpha}$ and a reference direction, in this case the direction of $\mathbf{e}_1$. The orientation is periodic with period π and is here defined in the interval $[-\pi/2, \pi/2)$.

The Schmid tensor $\mathbf{t}^{(k)}$ of slip system k is a geometric description of the slip system defined by $\mathbf{t}^{(k)} = \mathbf{s}^{(k)} \otimes \mathbf{n}^{(k)}$, $k = 1, 2$. The components of this tensor can be expanded in terms of the geometric descriptors of the crystal to give

$$[\mathbf{t}^{(k)}] = \frac{1}{2}\begin{bmatrix} -\cos(\phi + c^{(k)}\theta)\sin(\phi + c^{(k)}\theta) & \cos^2(\phi + c^{(k)}\theta) \\ -\sin^2(\phi + c^{(k)}\theta) & \sin(\phi + c^{(k)}\theta)\cos(\phi + c^{(k)}\theta) \end{bmatrix}, \tag{1}$$

where $c^{(1)} = 1$ and $c^{(2)} = -1$. Decomposition of $\mathbf{t}^{(k)}$ yields symmetric and skew tensors $\mathbf{p}^{(k)}$ and $\mathbf{q}^{(k)}$, respectively, the components of which are

$$[\mathbf{p}^{(k)}] = \frac{1}{2}\begin{bmatrix} -\sin[2(\phi + c^{(k)}\theta)] & \cos[2(\phi + c^{(k)}\theta)] \\ \text{sym} & \sin[2(\phi + c^{(k)}\theta)] \end{bmatrix}, \tag{2}$$

$$\text{and} \qquad [\mathbf{q}^{(k)}] = \frac{1}{2}\begin{bmatrix} 0 & 1 \\ -1 & 0 \end{bmatrix}.$$

2.3. External action

The action on the crystals is specified in terms of the velocity gradient tensor $\mathbf{l}$. Let $\mathbf{v}(\mathbf{x})$ be the velocity at a point $\mathbf{x}$ in the crystal, that is, the time rate of change of the motion applied to the material at $\mathbf{x}$. The velocity gradient tensor $\mathbf{l}$ is given by $l_{ij} = \partial v_i/\partial x_j$, $i, j = 1, 2$. The components of $\mathbf{l}$ are constrained by the assumption that no elastic deformation occurs in the material. The two-dimensional deformation must therefore preserve areas, that is, $l_{11} = -l_{22}$. Physically, the diagonal components of $\mathbf{l}$ are related to axial deformations, while the offdiagonal components relate to shear deformations.

Decomposition of the velocity gradient tensor $\mathbf{l}$ yields a symmetric tensor $\mathbf{d} = 1/2(\mathbf{l} + \mathbf{l}^{\mathrm{T}})$ and a skew tensor $\boldsymbol{\omega} = 1/2(\mathbf{l} - \mathbf{l}^{\mathrm{T}})$ which are called the deformation rate and spin, respectively. The spin tensor represents the part of the deformation which results in rigid body rotation of the material, while the deformation rate tensor represents the irrotational part of the applied deformation.

2.4. Derivation of orientation governing equation

The geometric parameters describing the crystal are now combined with the definition of the imposed action to arrive at a governing differential equation for the orientation. The derivation largely follows one given elsewhere [8], but the final result is expressed in a form more convenient for the current analysis.

Because there are only two active slip systems, there exists a unique combination of slip system shear rates which can accommodate the imposed inelastic deformation. The shear rates can therefore be found directly from the deformation parameters. If additional slip systems are introduced, many possible combinations of slip rates exist which accommodate the applied deformation, and an assumption regarding the constitutive behavior of the material must be introduced in order to determine the slip rates. The introduction of a constitutive model significantly complicates the analysis. The slip system shear rates when only two slip systems are present can be obtained by solution of the linear algebraic equations

$$\mathbf{d} : \mathbf{p}^{(k)} = \sum_{k=1,2} \dot{\gamma}^{(l)} \mathbf{p}^{(l)} : \mathbf{p}^{(k)}, \tag{3}$$

in which $\mathbf{a} : \mathbf{b} = a_{ij} b_{ij}$ denotes the inner product of the tensors $\mathbf{a}$ and $\mathbf{b}$. This equation can be rewritten as the system of equations

$$\begin{bmatrix} d_{11} \\ d_{12} \end{bmatrix} = \dot{\gamma}^{(1)} \begin{bmatrix} p_{11}^{(1)} \\ p_{12}^{(1)} \end{bmatrix} + \dot{\gamma}^{(2)} \begin{bmatrix} p_{11}^{(2)} \\ p_{12}^{(2)} \end{bmatrix}, \tag{4}$$

which can be solved for the slip system shear rates. The solution obtained for the slip system shear rates is, in terms of the components of $\mathbf{p}$ and $\mathbf{d}$,

$$\dot{\gamma}^{(1)} = \frac{p_{12}^{(2)} d_{11} - p_{11}^{(2)} d_{12}}{p_{11}^{(1)} p_{12}^{(2)} - p_{12}^{(1)} p_{11}^{(2)}}, \quad \dot{\gamma}^{(2)} = \frac{p_{11}^{(1)} d_{12} - p_{12}^{(1)} d_{11}}{p_{11}^{(1)} p_{12}^{(2)} - p_{12}^{(1)} p_{11}^{(2)}}. \tag{5}$$

The slip system shear rates are now available in terms of the applied deformation and slip system geometry. The equation for the rate of change of the orientation vector is

$$\dot{\boldsymbol{\alpha}} = \boldsymbol{\omega}^l \boldsymbol{\alpha} = (\boldsymbol{\omega} - \boldsymbol{\omega}^p)\boldsymbol{\alpha}, \tag{6}$$

where $\boldsymbol{\omega}^l$ is the part of the applied spin which results in evolution of the orientation, and $\boldsymbol{\omega}^p$ is the part of the spin tensor resulting from sliding along the slip directions. The rate of change of the orientation angle is obtained from Eq. (6),

$$\dot{\phi} = \omega_{12} - \sum_{k=1,2} \dot{\gamma}^{(k)} q_{12}^{(k)} = \frac{l_{12} - l_{21}}{2} - \frac{1}{2} \sum_{k=1,2} \dot{\gamma}^{(k)}. \tag{7}$$

By substituting the components of $\mathbf{p}^{(k)}$ from Eq. (2) and $d_{11} = l_{11}$, $d_{12} = (l_{12} + l_{21})/2$ into Eq. (5), and then inserting the resulting expressions into Eq. (7), the final governing ordinary differential equation for the orientation is obtained. This equation is

$$\dot{\phi} = \frac{l_{12} - l_{21}}{2} - \frac{\sec(2\theta)}{2}[(l_{12} + l_{21})\cos(2\phi) - 2l_{11}\sin(2\phi)]. \tag{8}$$

3. Deterministic deformation

The governing equation for the orientation can be solved for certain deterministic deformations. These solutions illustrate some features and patterns of orientation evolution.

The dynamics of the orientation are shown in the $(\phi, \dot{\phi})$ phase space. The differential equation for ϕ may or may not have fixed points, defined by the condition $\dot{\phi} = 0$. At a fixed point the orientation does not change in time. The condition $\dot{\phi} = 0$ implies

$$\frac{l_{12} - l_{21}}{2} = \frac{\sec(2\theta)}{2}[(l_{12} + l_{21})\cos(2\phi) - 2l_{11}\sin(2\phi)]. \tag{9}$$

The right-hand side of Eq. (9) is a harmonic in ϕ with period π with a scaling factor dependent upon the value of the geometric parameter θ. Fixed points of the system can be stable, unstable, or semi-stable. If equilibrium point ϕ_e is stable then all trajectories $\phi(t)$ converge to ϕ_e for $\phi(0) \in [\phi_e - \epsilon, \phi_e + \epsilon]$ where $\epsilon > 0$ is a small number. If ϕ_e is unstable all trajectories $\phi(t)$ for $\phi(0) \in [\phi_e - \epsilon, \phi_e + \epsilon]$ diverge from ϕ_e, except for $\phi(0) = \phi_e$, which does not evolve. If ϕ_e is neutrally stable trajectories converge for $\phi(0) \in [\phi, \phi_e + \epsilon]$ and diverge for $\phi(0) \in [\phi_e - \epsilon, \phi]$ or vice versa.

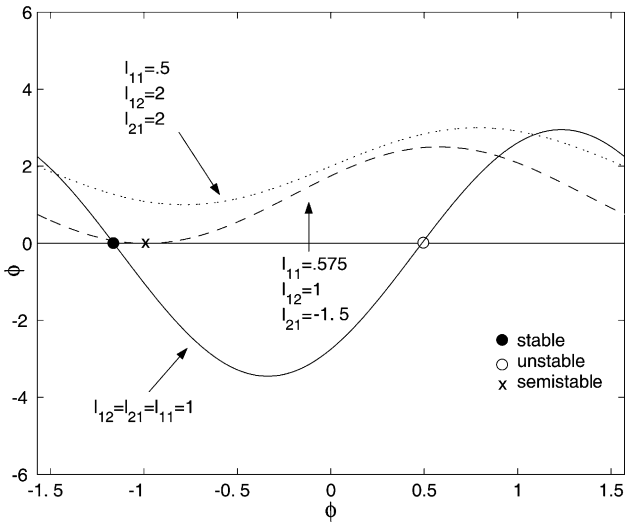

Fig. 4. Phase space diagram of the governing equation for orientation. The three possible scenarios of zero, one, or two fixed points of the system are illustrated.

Fig. 4 shows the three equilibrium conditions which are possible in the system: two fixed points, one stable and one unstable, a single, semi-stable fixed point, or no fixed points. The examples shown in the figure, as with all examples given in this paper, use the value $\theta = \pi/6$ without loss of generality.

The types of behavior shown in the phase space portrait of Fig. 4 can also be observed in plots of sample paths of the orientation as it evolves in time. Fig. 5 shows a series of three such illustrations, corresponding to the three cases described above. The sample paths in Fig. 5 were obtained by numerical integration of Eq. (8) with appropriate values of the velocity gradient components. The main observation regarding equilibrium solutions of the system is that except when $|l_{12} - l_{21}| \gg 0$ and $|l_{12} + l_{21}| \ll |l_{12} - l_{21}|$, almost all orientation paths tend to collect near a single orientation value. It is shown in later sections that this behavior does not necessarily hold when the applied deformations are allowed to be random.

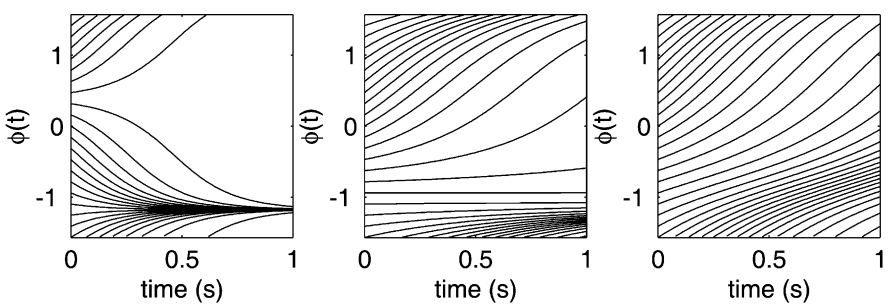

Fig. 5. Orientation sample paths for three deterministic deformations. From left to right: $l_{11} = l_{12} = l_{21} = 1$; $l_{11} = 0.575$, $l_{12} = 1$, $l_{21} = -1.5$; $l_{11} = 0.5$, $l_{12} = 2$, $l_{21} = -2$.

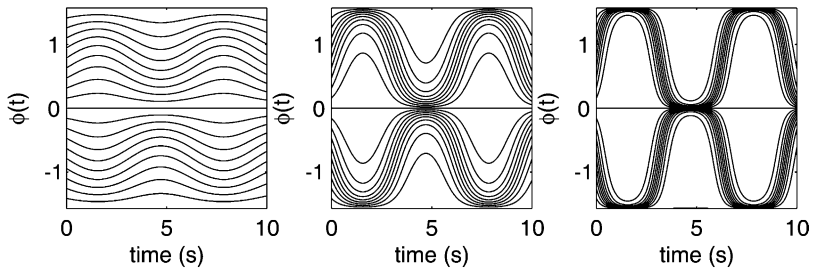

Fig. 6. Orientation sample paths for harmonic axial deformation with mean zero $l_{11}(t) = a\cos\omega t$, $l_{12}(t) = l_{21}(t) = 0$ with, from left to right, $a = 0.1, 0.5, 1.0$.

It is possible, for certain classes of applied deformations, to obtain closed form solutions to the governing ODE, Eq. (8). One of the simplest possible applied deformations is a monotonic axial strain. This deformation corresponds to a displacement field $u(x_1) = kx_1t$, where k is a constant and $u(\cdot)$ is the displacement in the x_1 direction. The resulting velocity is $\dot{u}(x_1) = kx_1$ and the resulting velocity gradient tensor has components $l_{11} = k$ and $l_{12} = l_{21} = 0$. In this case Eq. (8) reduces to $\dot{\phi} = k\sec 2\theta \sin 2\phi$, the solution to which is

$$\phi(t) = \operatorname{arccot}[\cot(\phi_0)\exp(-2kt\sec(2\theta)], \tag{10}$$

in which $\phi(0) = \phi_0$ is the initial condition. The solution has equilibrium points at $\phi = 0$ and $\phi = -\pi/2$. If $k > 0$, the equilibrium point at $\phi = 0$ is unstable, and those at $-\pi/2$ are stable. For $k < 0$ the stability of the equilibrium points reverses.

If the applied deformation consists solely of monotonic shearing, for example, $l_{11} = 0$, $l_{12} = -l_{21} = k$ the solution retains the same structure as for a monotonic axial deformation, with two equilibrium points, one stable and one unstable. The location of the equilibrium points is, however, shifted by $\pi/4$. The closed form solution is also obtained by applying a shift of $\pi/4$ to the solution for monotonic axial deformation. This solution is

$$\phi(t) = \operatorname{arccot}\left[\cot\left(\phi_0 + \frac{\pi}{4}\right)\exp(-2kt\sec(2\theta))\right] - \frac{\pi}{4}. \tag{11}$$

Let $l_{11}(t) = a\cos\omega t$, $l_{12}(t) = l_{21}(t) = 0$ so that the applied deformation is no longer monotonic, but rather harmonic. The solution to the resulting form of Eq. (8) is

$$\phi(t) = \operatorname{arccot}\left[\cot(\phi_0)\exp\left(-\frac{2a\sin(\omega t)}{\omega\cos(2\theta)}\right)\right], \tag{12}$$

which is itself periodic, though not harmonic. This solution is shown graphically in Fig. 6 for three values of the scaling parameter a, each with $\omega = 1$. An observation from Fig. 6 is that when the amplitude of the applied oscillatory deformation is small, the full range of possible values of the orientation is well represented at all times. On the other hand, when the deformation amplitude is large, the bulk of the orientation paths appear to reside mostly near the equilibrium points, which switch stability with the change in sign of the deformation parameter $l_{11}(t)$. This is evident in Figs. 7 and 8 which show estimates of the ODF at various time instants for $a = 0.1$ and 1.0. Comparison with Fig. 6 reveals that when the amplitude of the applied deformation is large, the ODF quickly evolves to a form which is nearly zero throughout much of the range of possible orientations.

The final deterministic solution to be examined is that of crystals subject to cyclic deformation with a non-zero mean. In the case of axial straining, the applied deformation is $l_{11}(t) = a_1 + a_2\cos(\omega t)$, $l_{12}(t) = l_{21}(t) = 0$, resulting in the solution

$$\phi(t) = \operatorname{arccot}\left[\cot(\phi_0)\exp\left(-\frac{2a_1t}{\cos(2\theta)} - \frac{2a_2\sin(\omega t)}{\omega\cos(2\theta)}\right)\right]. \tag{13}$$

Sample solutions are shown graphically in Fig. 9 for several values of the parameters a_1 and a_2. The solutions have an oscillatory part superimposed on a drift towards one of the equilibrium points. The equilibrium point towards

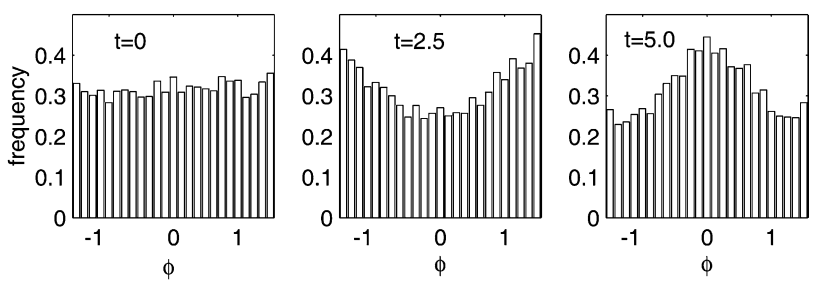

Fig. 7. Estimate of ODF at $t = 0, 2.5, 5.0$ for $L_{11} = a\cos\omega t$ with $a = 0.1$.

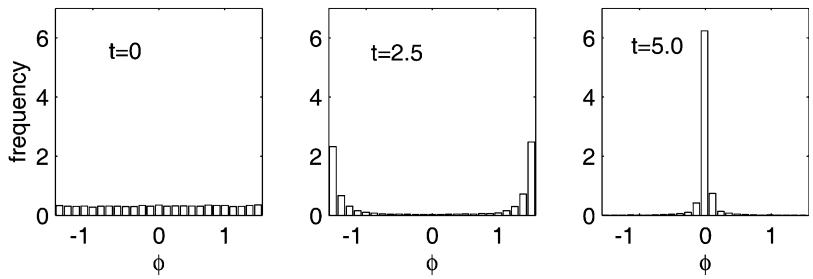

Fig. 8. Estimate of ODF at $t = 0, 2.5, 5.0$ for $L_{11} = a \cos \omega t$ with $a = 1.0$.

which the orientation paths drift is determined by the sign of a_1 as it was by the sign of k in the monotonic case described previously. Thus, even for a deformation which is not monotonic, but has a non-zero mean, nearly all initial orientations eventually approach a single value.

In summary, several observations of the behavior of the deterministic system will be useful reference points in the forthcoming discussion of the stochastic version of the system. For monotonic deformations, nearly all possible initial orientations eventually reorient to be near the stable or semi-stable equilibrium point of the system. Only applied deformations with large shear components of opposite sign result in systems with no equilibrium points. When the applied deformation is either a harmonic pure axial deformation or a harmonic pure shear deformation with zero mean, the resulting orientation paths are cyclic, but not harmonic. When a harmonic deformation is applied with non-zero mean, nearly all initial orientations evolve to be near the equilibrium point of the system which would be stable for a monotonic applied deformation of the same sign as the average value of the cyclic deformation. This evolution towards the equilibrium point need not, however, be monotonic, depending upon the relative amplitudes of the mean deformation and the harmonic part of the deformation.

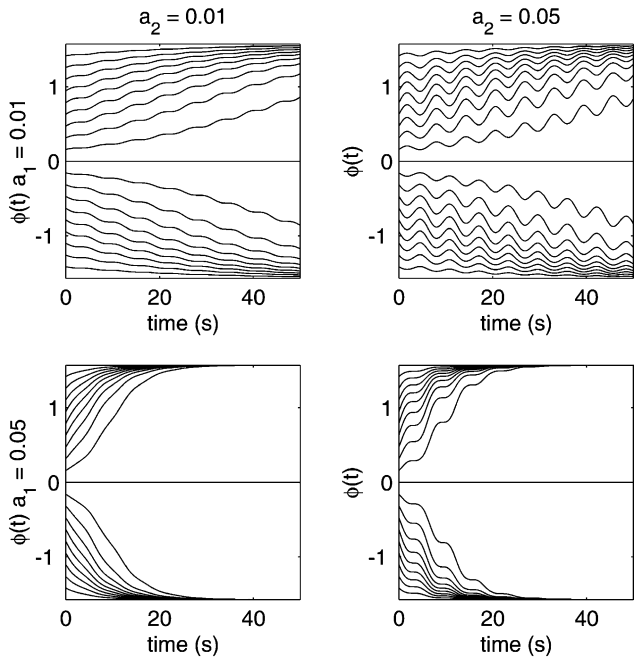

Fig. 9. Orientation sample paths for harmonic axial deformation with non-zero mean.

4. Random deformation

The governing differential equation for the orientation, Eq. (8) becomes the stochastic differential equation

$$\dot{\Phi}(t) = \frac{L_{12}(t) - L_{21}(t)}{2} - \frac{\sec(2\theta)}{2}[(L_{12}(t) + L_{21}(t))\cos(2\phi) - 2L_{11}(t)\sin(2\phi)], \tag{14}$$

when the components of the applied velocity gradient are assumed to be the random processes $L_{ij}(t)$, $i,j = 1,2$. Eq. (14) is identical to Eq. (8) except for the capitalization of the orientation and velocity gradient components to indicate that they are random quantities.

The objective here is to analyze the evolution of the probability density function of the orientation, or ODF, governed by Eq. (14). In investigating the evolution of the ODF, two methods are used, Monte Carlo simulation and solution of a Fokker-Planck equation for the time varying ODF. In the Monte Carlo simulations the governing differential equation is integrated numerically given realizations of the deformation processes $L_{ij}(t)$ to obtain realizations of the orientation process $\Phi(t)$. Estimates of the ODF at various stages of deformation can be obtained by which the evolution of the ODF can be analyzed. The ODF is the solution of a Fokker-Planck equation derived from Eq. (14). Solution of a Fokker-Planck equation is computationally efficient but can be achieved only for a class of processes L_{ij}.

4.1. Fokker-Planck equation

Let $\mathbf{X}(t)$ be an n-dimensional vector diffusion process defined by the stochastic differential equation

$$\mathrm{d}\mathbf{X}(t) = \mathbf{m}(\mathbf{x}, t)\mathrm{d}t + \boldsymbol{\sigma}(\mathbf{x}, t)\mathrm{d}\mathbf{B}(t), \tag{15}$$

where $\mathbf{m}(\mathbf{x}, t)$ is the $n \times 1$ vector drift function, $\boldsymbol{\sigma}(\mathbf{x}, t)$ is the $n \times n$ matrix diffusion function, and $\mathbf{B}(t)$ is an n-dimensional Brownian motion process, with $\mathrm{d}\mathbf{B}(t)$ being the increment of this process. The PDF of $\mathbf{X}(t)$, denoted by $f(\mathbf{x}, t)$ is, in

general, a function of time and initial conditions, and obeys the partial differential equation

$$\frac{\partial f}{\partial t} = -\sum_{i=1}^{n} \frac{\partial}{\partial x_i}[m_i(\mathbf{x},t)f] + \frac{1}{2}\sum_{i,j=1}^{n} \frac{\partial^2}{\partial x_i \partial x_j}[b_{ij}(\mathbf{x},t)f], \tag{16}$$

referred to as a Fokker-Planck equation, where $b_{ij}(\mathbf{x},t) = [\boldsymbol{\sigma}(\mathbf{x},t)\boldsymbol{\sigma}(\mathbf{x},t)^{\mathrm{T}}]_{ij}$.

Suppose that the components of the velocity gradient are arranged in a vector, $\hat{\mathbf{L}} = [L_{11}(t), L_{12}(t), L_{21}(t)]^{\mathrm{T}}$ and form a diffusion process defined by

$$\mathrm{d}\hat{\mathbf{L}} = \mathbf{m}(\hat{\mathbf{l}},t)\mathrm{d}t + \boldsymbol{\sigma}(\hat{\mathbf{l}},t)\mathrm{d}\mathbf{B}(t), \tag{17}$$

where $\mathbf{m}(\hat{\mathbf{l}})$ is a 3×1 vector drift function, $\boldsymbol{\sigma}(\hat{\mathbf{l}})$ is a 3×3 matrix diffusion function, and $\mathrm{d}\mathbf{B}(t)$ is the increment of a 3×1 Brownian motion process.

Since the equation governing orientation evolution (Eq. (8)) contains each of the components of the velocity gradient, a four-dimensional diffusion equation can be written which defines the deformation processes and governs the behavior of the orientation. This four-dimensional diffusion equation is, in its most general form

$$\mathrm{d}\begin{bmatrix} \Phi \\ \hat{\mathbf{L}} \end{bmatrix} = \begin{bmatrix} g(\phi,\hat{\mathbf{l}},t) \\ \mathbf{m}(\hat{\mathbf{l}},t) \end{bmatrix}\mathrm{d}t + \begin{bmatrix} 0 & 0 \\ 0 & \boldsymbol{\sigma}(\hat{\mathbf{l}},t) \end{bmatrix}\mathrm{d}\mathbf{B}(t), \tag{18}$$

where $\mathbf{m}(\hat{\mathbf{l}},t)$ and $\boldsymbol{\sigma}(\hat{\mathbf{l}},t)$ are as before, and $\mathbf{B}(t)$ is now a four-dimensional Brownian motion process. In Eq. (18), the function $g(\phi,\hat{\mathbf{l}},t)$, obtained from Eq. (8) is

$$g(\phi,\hat{\mathbf{l}},t) = \frac{l_{12}(t)-l_{21}(t)}{2} - \frac{\sec(2\theta)}{2}[(l_{12}(t)+l_{21}(t))\cos(2\phi) - 2l_{11}(t)\sin(2\phi)]. \tag{19}$$

The drift and diffusion functions of Eq. (18) can be substituted into the Fokker-Planck equation (Eq. (16)). In principle, the resulting Fokker-Planck equation can then be solved to obtain the time varying joint probability density function of the orientation and the three deformation processes. Analytical solutions of Fokker-Planck equations are available only in special cases. Approximate numerical solution of such equations is possible [15,16], requiring significant computing resources.

Certain assumptions are now introduced regarding the nature of the applied deformation processes. Two cases are examined. In the first, the deformation processes are assumed to be of the form

$$\begin{aligned} L_{11} &= \langle L_{11}\rangle + Q_1\frac{\mathrm{d}B_1(t)}{\mathrm{d}t}, \\ L_{12} &= \langle L_{12}\rangle + Q_2\frac{\mathrm{d}B_2(t)}{\mathrm{d}t}, \\ L_{21} &= \langle L_{21}\rangle + Q_3\frac{\mathrm{d}B_3(t)}{\mathrm{d}t}, \end{aligned} \tag{20}$$

in which $\langle L_{ij}\rangle$ represents the mean value of deformation process $L_{ij}(t)$, and the coefficients Q_i are constant scaling factors applied to the Gaussian white noise process denoted by the formal derivatives $\mathrm{d}B_i(t)/\mathrm{d}t$ of the Brownian motion processes $B_i(t)$ which are mutually independent. Substitution of Eq. (20) into Eq. (8) results in the diffusion equation

$$\begin{aligned} \mathrm{d}\Phi = &\left[\frac{\langle L_{12}\rangle - \langle L_{21}\rangle}{2} - [(\langle L_{12}\rangle + \langle L_{21}\rangle)\cos(2\phi) - 2\langle L_{11}\rangle\sin(2\phi)]\right]\mathrm{d}t - 2Q_1\sin(2\phi)\mathrm{d}B_1(t) \\ &+ Q_2[\tfrac{1}{2} - \cos(2\phi)]\mathrm{d}B_2(t) - Q_3[\tfrac{1}{2} + \cos(2\phi)]\mathrm{d}B_3(t). \end{aligned} \tag{21}$$

The drift function in this case is

$$m(\phi) = \left[\frac{\langle L_{12}\rangle - \langle L_{21}\rangle}{2} - [(\langle L_{12}\rangle + \langle L_{21}\rangle)\cos(2\phi) - 2\langle L_{11}\rangle\sin(2\phi)]\right]. \tag{22}$$

The matrix diffusion function in this case reduces to the 1×3 vector diffusion function

$$\boldsymbol{\sigma}(\phi) = [-2Q_1\sin(2\phi), Q_2(\tfrac{1}{2} - \cos(2\phi)), -Q_3(\tfrac{1}{2} + \cos(2\phi))]. \tag{23}$$

These drift and diffusion functions can be substituted into Eq. (16) to obtain the Fokker-Planck equation governing the evolution of the ODF for a crystal subject to deformations given by Eq. (20).

In the above discussion, the three deformation processes, $L_{11}(t)$, $L_{12}(t)$, $L_{21}(t)$ have random parts which are independent of one another. An alternative is the case where the random parts of the deformation process are proportional to one another. One possible form of such deformation processes, analogous to that of Eq. (20) is

$$\begin{aligned} L_{11}(t) &= \langle L_{11}\rangle + Q_1\frac{\mathrm{d}B(t)}{\mathrm{d}t}, \\ L_{12}(t) &= \langle L_{12}\rangle + Q_2\frac{\mathrm{d}B(t)}{\mathrm{d}t}, \\ L_{11}(t) &= \langle L_{21}\rangle + Q_3\frac{\mathrm{d}B(t)}{\mathrm{d}t}, \end{aligned} \tag{24}$$

where the coefficients Q_i are again constant scaling factors applied to the Gaussian white noise processes which are identical. Substitution of Eq. (24) into Eq. (8) yields a diffusion equation for the orientation with

$$m(\phi) = \left[\frac{\langle L_{12}\rangle - \langle L_{21}\rangle}{2} - [(\langle L_{12}\rangle + \langle L_{21}\rangle)\cos(2\phi) - 2\langle L_{11}\rangle\sin(2\phi)]\right], \tag{25}$$

and

$$\sigma(\phi) = \left[\frac{Q_2 - Q_3}{2} - [(Q_2 + Q_3)\cos(2\phi) - 2Q_1 \sin(2\phi)] \right]. \tag{26}$$

5. Results

Results are presented regarding the evolution of the ODF in crystals subject to random deformation. First, a closed form stationary solution to the Fokker-Planck equation is presented for the case of an applied deformation which is purely axial. Second, the Fokker-Planck equation is solved numerically using the first order finite difference method for a variety of values of the deformation parameters $\langle L_{11} \rangle$, $\langle L_{12} \rangle$, $\langle L_{21} \rangle$, Q_1, Q_2, Q_3. Results of Monte Carlo simulations are also shown for certain cases not amenable to analysis using the Fokker-Planck equation.

5.1. Analytic results

If a stationary PDF exists for a scalar diffusion process $X(t)$, it can be calculated using [17]

$$f(x) = \frac{q_2}{b(x)} \exp\left[2 \int_0^x \frac{m(u)}{b(u)} \mathrm{d}u \right] - \frac{2q_1}{b(x)} \int_0^x \exp\left[2 \int_u^x \frac{m(v)}{b(v)} \mathrm{d}v \right] \mathrm{d}u, \tag{27}$$

where $b(x) = \boldsymbol{\sigma}\boldsymbol{\sigma}^{\mathrm{T}}\, m(x)$ is the drift function, and q_1, q_2 are constants. The unknown constants can be found by use of prescribed boundary conditions on $f(x)$ and by the normalization condition $\int_{-\infty}^{\infty} f(x)\mathrm{d}x = 1$.

Assuming a deformation of the form given by Eq. (24) and setting $\langle L_{11} \rangle = A$ and $Q_1 = B$ with $\langle L_{12} \rangle = \langle L_{21} \rangle = Q_2 = Q_3 = 0$, the stationary solution to Eq. (16)

$$f(\phi) = \begin{cases} \delta(\phi - \pi/2), & A/B^2 \neq 0, \\ \frac{1}{2}(\delta(\phi - \pi/2) + \delta(\phi)), & A/B^2 = 0, \end{cases} \tag{28}$$

where $A > 0$ has been assumed without loss of generality. This solution has some interesting features. First, according to this solution, as long as the applied velocity gradient has non-zero mean, all orientation paths eventually flow to $\phi = \pi/2$, regardless of the scale of the random part of the deformation process. This is surprising, as intuition might suggest that the introduction of a random part to the deformation process would result in a stationary ODF with non-zero variance, but this is apparently not the case. Even when the mean of the deformation process is zero, that is $A/B^2 = 0$, the ODF evolves into a function comprising two delta functions. This is again surprising as intuition would suggest that a mean zero random deformation process would result in a stationary ODF with non-zero values throughout the range $(-\pi/2, \pi/2]$.

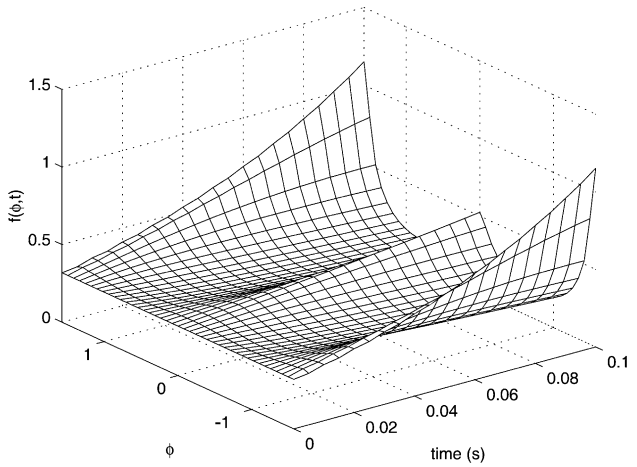

Fig. 10. Finite difference solution to the Fokker-Planck equation for orientation for an axial applied deformation with $\langle L_{11} \rangle = 1.0$ and $Q_1 = 0.75$.

5.2. Fokker-Planck solutions and Monte Carlo simulation

The Fokker-Planck equation is solved approximately using a first-order finite difference approximation for a variety of axial, shear, and mixed mode deformations. In all results presented in this section the initial condition of the ODF has been taken to be uniform, that is, $f(\phi) = 1/\pi$, $\phi \in [-\pi/2, \pi/2)$.

Consider first the case of a purely axial deformation with $\langle L_{11} \rangle = 1$ and $Q_1 = 0.75$. The result of the finite difference calculation is shown in Fig. 10. The results show clearly that starting from an initially uniform ODF, orientations initially accumulate near the fixed points of the system at $0, -\pi/2$, with probability mass accumulating at a greater rate near $-\pi/2$. In accordance with the stationary solution given in the previous section, eventually all orientation paths must approach $-\pi/2$ for the parameters used in this example. This behavior has not yet been observed in the finite difference solution. As can

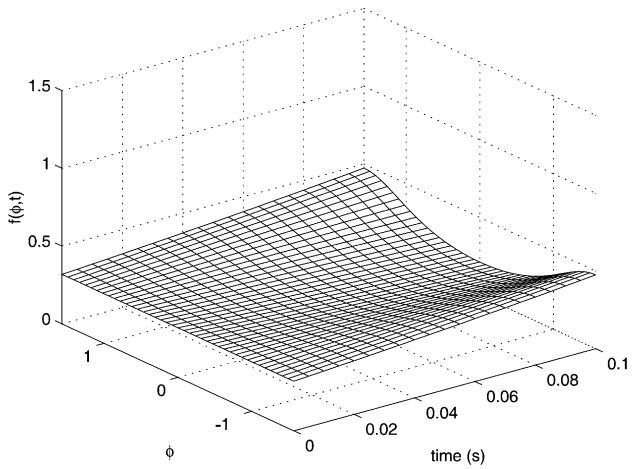

Fig. 11. Finite difference solution to the Fokker-Planck equation for orientation for a deterministic axial applied deformation with $\langle L_{11} \rangle = 1.0$ and $Q_1 = 0$.

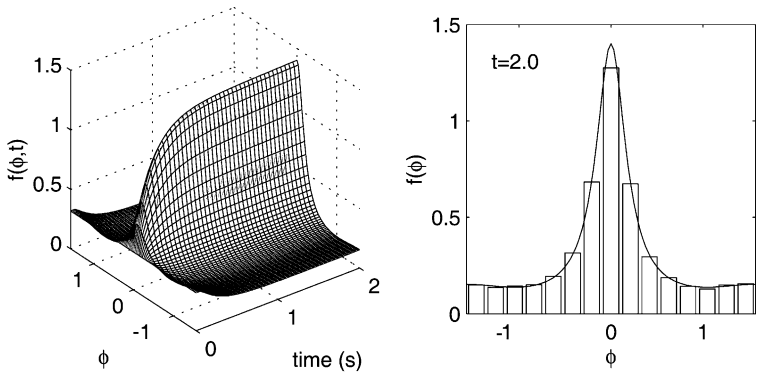

Fig. 12. Fokker-Planck solution for $\langle L_{11}\rangle = \langle L_{12}\rangle = \langle L_{21}\rangle = 0$ and $Q_i = 1.0$. Note the establishment of an apparently stationary ODF before $t = 1.0$. Also, a comparison of the Fokker-Planck solution with the results of Monte Carlo simulation.

be seen in the figure, the gradients of $f(\phi, t)$ become large quite quickly. Accurate solution of the Fokker-Planck equation into the time ranges when such behavior would be expected to occur requires a very fine discretization beyond the capabilities of computing resources available to the authors. Fig. 11 shows the solution to the Fokker-Planck equation with $\langle L_{11}\rangle = 1$, $Q_1 = 0$, that is, a deterministic deformation. Comparison of Figs. 10 and 11 shows that the introduction of randomness to the deformation process drives reorientation at a faster average rate.

When the applied deformation is purely axial, the numerical and analytic solutions presented previously indicate that a collection of crystals with an initially uniform, or highly heterogeneous microstructure, evolves towards a state in which only one or two orientations are represented; a state of increased homogeneity. From results for deterministic deformations presented in Section 3, it would be expected that the behavior would be similar for pure shear deformations, with only the location of the equilibrium points shifted. When the applied deformation is a mixed mode, random deformation, however, it is possible for the system to evolve to a stationary ODF which represents a significant preservation of heterogeneity.

Let $Q_1 = Q_2 = Q_3 = 1$ with all other deformation parameters zero. Also, let the applied deformation be of the form of Eq. (24) so that the deformation processes have independent random parts. The time-varying ODF for this deformation is shown in Fig. 12. In the left-hand frame it can be seen that the ODF reaches stationarity. The right frame shows that the stationary ODF retains significant probability mass throughout the entire range of definition of ϕ. The histogram in the right figure represents the results of a Monte Carlo simulation with 10,000 samples. The agreement with the Fokker-Planck solution is satisfactory.

To illustrate the importance of interdependence between the random parts of the deformation process, Monte Carlo simulation has been used to analyze the case in which $Q_1 = Q_2 = Q_3 = 1$ but the deformation processes follow the form of Eq. (20), that is, the random parts are proportional to one another. In this case, since $Q_1 = Q_2 = Q_3$ and $\langle L_{11}\rangle = \langle L_{12}\rangle = \langle L_{21}\rangle = 0$, the deformation processes are identical. The results of the Monte Carlo simulation of 10,000 samples are shown in Fig. 13 and show clearly the different character of the solution. Whereas when the deformation processes are independent, a stationary ODF is obtained which has significant probability mass throughout the range $[-\pi/2, \pi/2)$, when the deformation processes are identical, the ODF evolves to a form in which it appears only two orientations are possible.

This previous example is not given to indicate, however, that no significant heterogeneity can be preserved when the random parts of the deformation are proportional. Fig. 14 shows the time-varying ODF for $\langle L_{11}\rangle = Q_2 = Q_3 = 1$ with all other deformation parameters zero and the random parts of the deformation process proportional as in Eq. (20). The ODF evolves to a stationary form which retains significant heterogeneity.

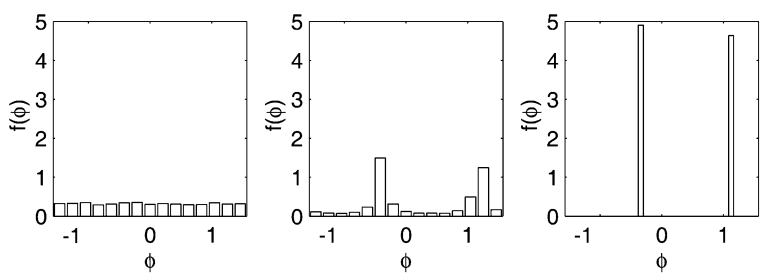

Fig. 13. Results of Monte Carlo simulation for $Q_i = 1.0$ and perfect dependence among the deformation processes. Results based on 10,000 realizations.

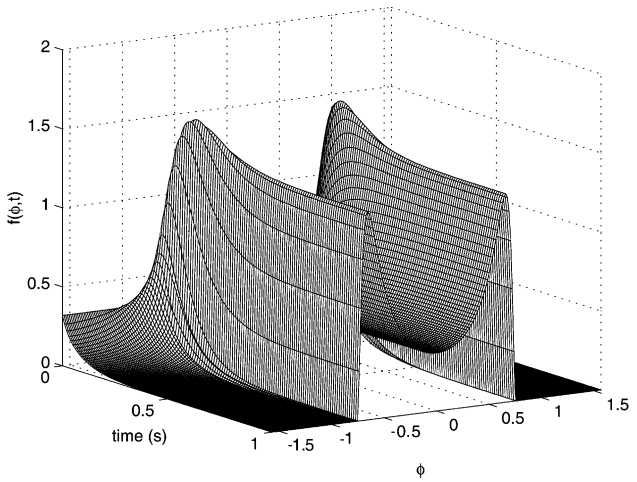

Fig. 14. A stationary ODF which is non-zero over a broad range of values can be obtained even when the random parts of the applied deformation are perfectly correlated. In this case, $\langle L_{11} \rangle = Q_2 = Q_3 = 1$.

6. Discussion and conclusions

The evolution of the probability density function of crystallographic orientation, the ODF, has been analyzed for aggregates of polycrystals subject to deterministic and random deformation. The physical system analyzed is highly simplified from the physically realistic case in order to permit the addition of increased complexity to the problem in the form of deformation randomness.

The crystals studied are assumed to be planar and infinite, and to have only two active slip systems, which accommodate any applied deformation entirely through plastic slip. In line with previous analysis of this same system subject to deterministic deformation, an ordinary differential equation has been derived which governs the evolution of the angle of orientation ϕ. For all monotonic deformations except extreme shear deformations, the orientation approaches a single value regardless of its initial value. When the applied deformation is harmonic with mean zero, the response orientation process is cyclic, though not harmonic. When a non-zero mean harmonic deformation is applied to the crystals, all orientations again approach a single value.

The governing equation for the orientation is rendered a stochastic differential equation when the applied deformation processes are assumed to themselves be random processes. When the applied deformations are diffusion processes the ODF is the solution of a Fokker-Planck equation. If the applied deformation processes take the form of a scaled Gaussian white noise process plus a constant mean value, the diffusion equation and corresponding Fokker-Planck equation for orientation can be solved either in closed form or approximately using the finite difference method.

For pure axial or shear deformations with zero temporal mean applied to the crystals all orientation paths approach one of two values. This evolution occurs despite the absence of a mean deformation component. When the applied deformation is either purely axial or pure shear but with a non-zero mean, all orientation paths approach a single value, consistent with the deterministic result. It appears that in all cases when the aggregate of crystal is subject to pure shear or axial deformations, a microstructure which is initially highly heterogeneous (e.g. a uniform ODF), evolves towards a state of increased homogeneity, with one, or at most two possible orientations remaining.

When a mixed mode deformation, that is, one with both axial and shear components, is applied it is possible for the polycrystal to retain significant heterogeneity of orientation. In the examples shown, the ODF evolves towards a stationary form which has significant non-zero values throughout a significant portion of the range of definition of the orientation angle, if not the entire range.

Acknowledgements

The authors would like to thank Professor P.R. Dawson of Cornell University for valuable discussions. Portions of this work were supported by the Air Force Office of Scientific Research under grant #F49620-98-1-0401.

References

[1] Beaudoin AJ, Dawson PR, Mathur KK, Kocks UF, Korzekwa DA. Application of polycrystal plasticity to sheet forming. Comput Meth Appl Mech Engng 1994;117:49–70.
[2] Beaudoin AJ, Dawson PR, Mathur KK, Kocks UF. A hybrid finite element formulation for polycrystal plasticity with consideration of macrostructural and microstructural linking. Int J Plast 1995;11:501–21.
[3] Dawson PR. Computational crystal plasticity. Int J Solids Struct 2000;37:115–30.
[4] Kumar A, Dawson PR. Polycrystal plasticity modeling of bulk forming with finite elements over orientation space. Comput Mech 1995;17:10–25.
[5] Kumar A, Dawson PR. Modeling crystallographic texture evolution with finite elements over neo-Eulerian orientation spaces. Comput Meth Appl Mech Engng 1998;153:259–302.
[6] Marin EB, Dawson PR. On modelling the elasto-viscoplastic response of metals using polycrystal plasticity. Comput Meth Appl Mech Engng 1998;165:1–22.
[7] Marin EB, Dawson PR. Elastoplastic finite element analysis of metal deformations using polycrystal constitutive models. Comput Meth Appl Mech Engng 1998;165:23–41.
[8] Prantil VC, Jenkins JT, Dawson PR. An analysis of texture and plastic spin for planar polycrystals. J Mech Phys Solids 1993;41:1357–82.
[9] Sarma GB, Dawson PR. Effects of interactions among crystals on the inhomogeneous deformations of polycrystals. Acta Metall Mater 1996;44:1937–53.
[10] Sarma GB, Dawson PR. Texture predictions using a polycrystal plasticity model incorporating neighbor interactions. Int J Plast 1996;12:1023–54.

[11] Avlonitis M, Zaiser M, Aifantis EC. Some exactly solvable models for the statistical evolution of internal variables during plastic deformation. Probab Engng Mech 2000;15:131–8.
[12] Aifantis EC. From micro- to macro-scale plasticity: the scale invariant approach. Trans ASME 1995;117:352–5.
[13] Ning J, Aifantis EC. Anisotropic yield and plastic flow of polycrystalline solids. Int J Plast 1996;12:1221–40.
[14] Randle V. The measurement of grain boundary geometry. Bristol, UK: Institute of Physics; 1993.
[15] Wojtkiewicz SF, Bergman LA, Spencer BF, Johnson EA. Numerical solution of the four dimensional non-stationary Fokker-Planck equation. In: Narayanan S, Iyengar R, editors. Nonlinearity and stochastic structural dynamics. ; 2001. p. 277–88.
[16] Wojtkiewicz SF, Bergman LA, Spencer BF. Numerical solution of some three-state random vibration problems. In: Proceedings of the 1995 ASME Design Engineering Technical Conference, Boston: ASME; 1995. p. 939–47.
[17] Soong TT, Grigoriu M. Random vibrations of mechanical and structural systems. Englewood Cliffs, NJ: Prentice Hall; 1993.
[18] Turner TJ. Personal communication; 1998.